Structure, Vol. 12, 1937–1945, November, 2004, ©2004 Elsevier Ltd. All rights reserved. DOI 10.1016/j.str.2004.08.009

Estriol Bound and Ligand-free Structures of Sterol 14α-Demethylase

Larissa M. Podust,[1,*] Liudmila V. Yermalitskaya,[1] Galina I. Lepesheva,[1] Vladimir N. Podust,[2] Enrique A. Dalmasso,[2] and Michael R. Waterman[1]
[1]Department of Biochemistry
Vanderbilt University School of Medicine
Nashville, Tennessee 37232
[2]Ciphergen Biosystems, Inc.
6611 Dumbarton Circle
Fremont, California 94555

Summary

Sterol 14α-demethylases (CYP51) are essential enzymes in sterol biosynthesis in eukaryotes and drug targets in antifungal therapy. Here, we report CYP51 structures in ligand-free and estriol bound forms. Using estriol as a probe, we determined orientation of the substrate in the active site, elucidated protein contacts with the invariant 3β-hydroxy group of a sterol, and identified F78 as a key discriminator between 4α-methylated and 4α,β-dimethylated substrates. Analysis of CYP51 dynamics revealed that the C helix undergoes helix-coil transition upon binding and dissociation of a ligand. Loss of helical structure of the C helix in the ligand-free form results in an unprecedented opening of the substrate binding site. Upon binding of estriol, the BC loop loses contacts with molecular surface and tends to adopt a closed conformation. A mechanism for azole resistance in the yeast pathogen *Candida albicans* associated with mutations in the ERG11 gene encoding CYP51 is suggested based on CYP51 protein dynamics.

Introduction

Sterol biosynthesis is primarily a eukaryotic process and is almost completely absent in prokaryotes. Essentially all eukaryotic cells use steroids in order to control the fluidity and flexibility of their cell membranes (Ourisson and Nakatani, 1994), and many cells use them as precursors of hormones and other biologically active compounds. The committed biosynthesis of steroids starts from squalene, a linear precursor that in the first step undergoes epoxidation catalyzed by squalene monooxygenase. Cyclization of squalene epoxide to form the initial sterol proceeds through the action of oxidosqualene cyclase. A variety of further reactions lead to different cyclic triterpenes, such as lanosterol in yeast and animals, eburicol in filamentous fungi, and obtusifoliol in plants. All are substrates in the next step of the sterol biosynthetic pathway, oxidative removal of the 14α-methyl group by cytochrome P450 sterol 14α-demethylase (CYP51), which leads to membrane sterols in animals (cholesterol), fungi (ergosterol), and plants (phytosterols).

CYP51 is widely distributed throughout all biological kingdoms from bacteria to animals and could be the most ancient family of cytochrome P450 monooxygenases (P450) (Aoyama et al., 1996). Being a key enzyme of sterol biosynthesis in fungi, plants, and animals, CYP51 has been a target for antifungal drug design for decades (Sheehan et al., 1999). Azole inhibitors are currently the most widely used and studied class of antifungal agents. Antifungal efficacy of azoles is attributed to their greater affinity for fungal CYP51 than for the mammalian enzyme (Koltin and Hitchcock, 1997). Use of standard antifungal therapies is limited for a number of reasons, including toxicity, low efficacy rates, and drug resistance, forcing the development not only of new triazole agents with enhanced potency, but also the introduction of new classes of antifungal drugs (Gupta and Tomas, 2003).

The occasional presence of sterols in bacteria is poorly understood. Sterol production by bacteria has been demonstrated in three groups of prokaryotes, *Methylococcales* (Bird et al., 1971; Schouten et al., 2000), *Myxobacteriales* (Bode et al., 2003; Kohl et al., 1983), and planctomycete *Gemmata obscuriglobus* (Pearson et al., 2003). *Mycobacterium tuberculosis* does not use sterols to build its cell envelope (Brennan and Nikaido, 1995), and it is not known to produce sterols, which is not surprising since squalene monooxygenase and oxidosqualene cyclase, required to form the initial sterol, are absent in the *M. tuberculosis* genome. However, the *M. tuberculosis* genome encodes a CYP51-like P450 having a sequence identity of 29%–39% with CYP51 genes in animals, plants, and fungi (Aoyama et al., 1998) and 49% identity with CYP51 from the proteobacterium *Methylococcus capsulatus* (Jackson et al., 2002), in which sterol biosynthesis is known (Bird et al., 1971). A CYP51-like gene was also identified in other pathogens from genus *Mycobacterium*, including *Mycobacterium avium* and *Mycobacterium bovis*, and in the nonpathogenic species *Mycobacterium smegmatis*. An aromatic-degrading bacterium from deep-terrestrial-subsurface sediments, *Novosphingobium aromaticivorans*, also contains a CYP51-like gene.

The crystal structure of MTCYP51 was determined for azole inhibitor bound forms (Podust et al., 2001a) and has remained the only structure for this important family of enzymes. Eukaryotic CYP51s are membrane associated proteins and represent a challenge for structural and biophysical characterization. The MTCYP51 structure revealed a most unusually shaped P450. Wide-open access to the active site is created by the disrupted and bent I helix and extended conformation of the BC loop. The structure also revealed a binding mode for azole inhibitors 4-phenylimidazole and the clinically important fluconazole, although the natural substrate binding mode has remained obscure.

Current research is aimed at elucidation of specificity of substrate binding in the CYP51 family. Since structural differences between substrates undergoing 14α-demethylation are small and local, the difference in substrate specificity is likely caused by only a few amino acid

*Correspondence: larissa.m.podust@vanderbilt.edu

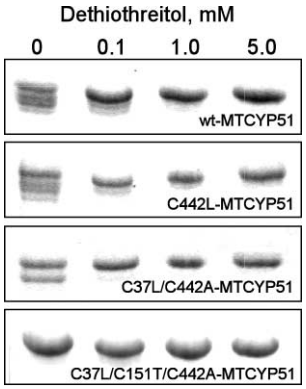

Figure 1. Analysis of MTCYP51 by SDS-PAGE

Analysis by SDS-PAGE of *E. coli*-expressed MTCYP51, wild-type and mutants, upon nonreducing and reducing conditions.

differences in the substrate-recognition site. In the current study, estriol was used as a probe for the substrate binding site of MTCYP51. The estriol bound 1.5 Å MTCYP51 structure unequivocally defined the orientation of the sterol in the active site. It also established that residue F78 is a key discriminator between CYP51 substrates that are singly versus doubly methylated at position C-4. The ligand-free 2.0 Å MTCYP51 structure revealed a further opening from the protein surface to the heme due to helix-coil transition in the C helix. Comparison of estriol bound and ligand-free forms of MTCYP51 indicates that binding of estriol in the active site induces remodeling of the C helix and the BC loop, which tend to enclose the sterol within the active site. The dynamics of MTCYP51 provide insights into the molecular basis of the mechanism of azole resistance in the yeast pathogen *Candida albicans* due to mutations in the CYP51 drug target.

Results and Discussion

Protein Design

Analysis by SDS-PAGE of MTCYP51 after purification from an *Escherichia coli* expression system revealed that in nonreducing conditions the protein migrates as a number of conformers of different mobility (Figure 1). This effect diminishes and disappears with increasing concentrations of DTT in the sample buffer, which apparently breaks intramolecular disulfide bonds formed between cysteine residues in MTCYP51. Since no disulfide bonds are present in folded MTCYP51 (Podust et al., 2001a), it is assumed that their formation occurs as a result of misfolding of a fraction of the protein during heterologous expression. As has been shown earlier (Lepesheva et al., 2001), folding of MTCYP51 in *E. coli* does not occur until almost the entire coding sequence is translated. Although not investigated in the current work, MTCYP51 might fold in *E. coli* via a path promoted by chaperonins GroEL/S (Houry et al., 1999). Proteins following this pathway fold slowly and are prone to aggregation (Gottesman and Hendrickson, 2000). Slow folding with formation of aggregates would allow cysteine residues to interact with each other with random

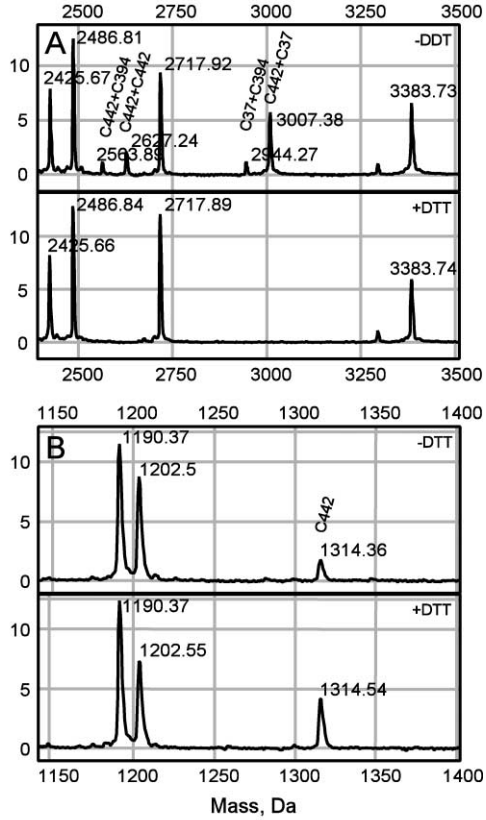

C

Mass, Da	Position	Peptide sequence
1694.8799	33-48	VRDE<u>C</u>GDVGTFQLAGK
1251.5678	394-405	<u>C</u>VGAAFAIMQIK
1314.6271	433-444	MVVQLAQPA<u>C</u>VR

1314.62 + 1251.56 - 2 = 2563.18 (2563.89)
1314.62 + 1314.62 - 2 = 2627.24 (2627.24)
1251.56 + 1694.87 - 2 = 2944.43 (2944.27)
1314.62 + 1694.87 - 2 = 3007.49 (3007.38)

Figure 2. Analysis of MTCYP51 Tryptic Digests by SELDI-TOF Mass Spectrometry

(A and B) Localization of the DTT-sensitive MTCYP51 tryptic digest peaks corresponding to (A) the crosslinks between MTCYP51 tryptic peptides containing cysteine residues, and (B) the C442-containing tryptic fragment showing a doubling in peak intensity upon reduction. (C) Theoretical masses of MTCYP51 tryptic fragments containing cysteine, and calculated and experimental (in parentheses) masses for disulfide crosslinks.

and spontaneous formation of disulfide bonds. The misfolded portion of MTCYP51 copurifies with the correctly folded protein through all three chromatographic steps.

Analysis of tryptic digests of purified MTCYP51 by SELDI-TOF mass spectrometry showed four major DTT-sensitive peaks (Figure 2A), each corresponding to a putative sum of two predicted tryptic fragments containing cysteine (Figure 2C). Interpretation of masses for DTT-sensitive ions leads to the conclusion that three of the four peaks contain the 1314.62 Da fragment with cysteine at position 442 (C442), including intermolecular crosslinking between two C442-containing fragments. Intensity of the peak corresponding to the C442 frag-

Table 1. Summary of Crystallographic Statistics

Crystal	Ligand-free	Estriol Bound
Space group	$P2_12_12_1$	$P2_12_12_1$
Unit cell	46.49/84.83/110.03	47.16/84.52/110.81
Data Collection		
Wavelength	1.5418	1.0000
Resolution (Å)[a]	40–2.05 (2.12–2.05)	50–1.55 (1.61–1.55)
Total/unique observations	103,288/25,277	264,701/63,041
Completeness (%)	90.6 (90.9)	96.7 (85.3)
Average I/σ	10.6 (3.1)	31.6 (3.0)
Redundancy	4.1 (3.1)	4.2 (3.2)
R_{sym}[b]	0.105 (0.457)	0.073 (0.37)
Refinement Statistics		
R_{crys}/R_{free} (%)[c]	18.5/23.6	20.6/22.7
Rms deviation		
Bonds (Å)	0.006	0.006
Angles (°)	1.2	1.2
Model Statistics		
Protein atoms	3437	3418
Ligand atoms	43	85
Solvent molecules	280	323
Ramachandran (%)[d]	90.1/9.7/0.3	92.2/7.5/0.3

[a] Values for highest-resolution shells are in parentheses.
[b] $R_{sym} = \Sigma|I_i - \langle I\rangle|/\Sigma\langle I\rangle$, in which $\langle I\rangle$ is the mean intensity of reflection.
[c] $R_{cryst} = \Sigma||F_0| - |F_c||/\Sigma|F_0|$, calculated with the working reflection set. R_{free} is the same as R_{cryst} but calculated with the reserved reflection set.
[d] Program PROCHECK (Laskowski et al., 1993).

ment itself increases approximately 2-fold upon DTT treatment (Figure 2B), suggesting that about half of the total C442 cysteine residues in the protein preparation are involved in Cys-Cys bridge formation, which coincides with the fraction of the protein containing heme in the P450 form as estimated by heme content assay (not shown). These facts lead to the conclusion that crosslinked misfolded protein species do not incorporate heme, and thus only half of the protein in the preparation is folded properly, resulting in inconsistency in crystal growth from one protein batch to another and failure in obtaining sterol bound crystals. To eliminate or at least to reduce this effect, three of the four MTCYP51 cysteines, C37, C151, and C442, were mutated to leucine, threonine, and alanine, respectively. These substitutions were chosen empirically by expression of mutated species followed by recording of CO-reduced difference spectra and monitoring of absorbance at 450 nm. Mutants showing more abundant expression based on this criterion were selected. C151 is the most sensitive of these three positions for mutagenesis, since its substitution to alanine, leucine, or serine resulted in complete or almost complete loss of absorption at 450 nm.

On SDS-PAGE, the C442A-MTCYP51 single mutant at nonreducing conditions migrates similar to the wild-type (Figure 1), as multiple bands with different mobility, while the C37L/C442A-MTCYP51 double mutant shows only one DTT-sensitive conformer, which apparently corresponds to a single crosslink between the two remaining cysteines in the protein sequence. The C37L/C151T/C442A-MTCYP51 triple mutant migrates as a single band independent of the presence of DTT. This observation indicates that disulfide bonds formed in MTCYP51 during heterologous expression and folding are nonspecific and might be a result of overloading of the *E. coli* molecular chaperone machinery. Work on crystallization and improvement of the protein construct developed in parallel. Therefore, the ligand-free crystals were obtained from the wild-type, and estriol bound crystals were obtained from the C37L/C442A-MTCYP51 double mutant a few years later (Table 1).

Estriol as a Probe for CYP51 Substrate Binding Site

The first attempts to cocrystallize MTCYP51 with the substrate lanosterol encountered two major problems: highly insoluble lanosterol and inconsistency in crystal growth from one protein batch to another. These attempts resulted in ligand-free crystals and failure to obtain crystals of the substrate bound form. To address the first problem, a number of more soluble sterols were tested in spectral protein binding assays. A few of them, estriol, androstenolone, and androstenedione, were found to bind to MTCYP51 with reasonable affinity, generating normal type I spectra characteristic of P450 substrate binding (Figure 3A). Estriol, having affinity of 100 μM versus 200 μM for androstenolone and androstenedione, was chosen as a probe for cocrystallization with MTCYP51. Estriol is not metabolized by MTCYP51 because of lack of the 14α-methyl group. Estriol also does not have methyl groups at positions C-4, C-10, and C-13, nor an aliphatic side chain at C-17. Instead, it is hydroxylated at C-16 and C-17, which makes it far more soluble then lanosterol and other CYP51 substrates (Figure 3B). Additionally, estriol ring planarity is altered compared to substrates due to different localization of the double bond(s). Taken together, these differences indicate that

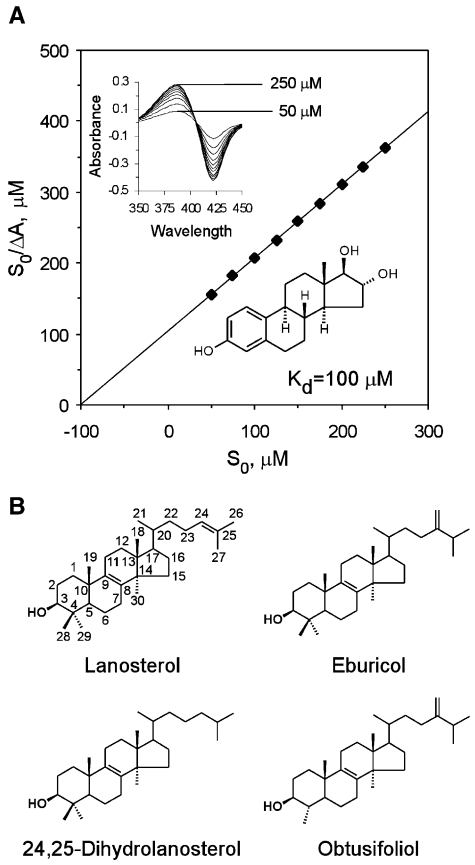

Figure 3. Estriol Binding by MTCYP51

(A) Type I binding spectra resulting from MTCYP51 titration with increasing concentrations of estriol ranging from 50 to 250 μM and linearization of the titration data.

(B) Endogenous CYP51 substrates. Steroid carbon nomenclature is shown for lanosterol.

the estriol binding mode would not be exactly the same as that for a more physiologic substrate; however, it does allow us to address issues such as (1) substrate orientation in the active site, (2) protein contacts with the invariant 3β-hydroxy group, and (3) the substrate selectivity in the CYP51 family toward discrimination between 4α-methylated and 4α,β-dimethylated substrates.

Ligand-free Structure

A prevailing view on substrate binding by cytochrome P450 is that the F and G helices and the loop connecting them undergo an open/close motion, which allows substrate to enter and product to be released. A number of bacterial CYPs (Park et al., 2002; Podust et al., 2003; Yano et al., 2000; Zerbe et al., 2002) and mammalian P4502B4 (Scott et al., 2003) demonstrate the wide range of openings available to the F-G region in P450s. However, flexibility of P450s seems not to be limited by the dynamics of the F-G region. Sterol metabolizing CYP51 is another example of an accessible active site, where the opening is generated by the break in the I helix and the extended conformation of the BC loop stretched over the protein surface. Although the FG channel is also apparent in the CYP51 structure, its entrance is closed at the surface. The ligand-free MTCYP51 structure determined in the current work revealed a surprising feature that has not previously been observed in P450s. In the ligand-free state, the C helix of MTCYP51 is disordered and no electron density is observed for residues 91–100. Although this helix is known to shift significantly in P4502B4 upon inhibitor binding (Scott et al., 2004), all large-scale conformational changes in P4502B4 are due to the relocation of structural elements toward each other with, according to the authors, remarkably little remodeling at the secondary structure level. Absence of the electron density for the C helix in the ligand-free MTCYP51 appears as a further opening of the heme binding pocket (Figure 4A). In contrast, in the 4-phenylimidazole bound structure, the C helix is well defined (Figure 4B), although temperature factors of residues constituting the helix are among the highest in the molecule (Figure 4C). Substitution of 4-phenylimidazole with fluconazole results in loss of the C helix helical structure, although continuous electron density persists.

Remodeling of the C Helix in MTCYP51 upon Ligand Binding

Interestingly, two estriol molecules are bound per one molecule of protein in the MTCYP51 structure. One is bound in the active site, while another binds in the hydrophobic crevice on the protein surface formed by the C and the H helices and the N terminus of the I helix, close to the active site entrance (Figure 4A), via purely hydrophobic interactions. Currently, it is impossible to distinguish whether binding of the second sterol molecule would have functional meaning or is an artifact of crystallization and crystal packing, since its contacts with the symmetrically related protein molecule are quite extensive.

Analysis of the MTCYP51 structure in its estriol bound form supports our previous assumption that MTCYP51 undergoes conformational changes upon binding of substrate in the active site (Podust et al., 2001a; Podust et al., 2001b). In the ligand-free form, the C helix and the C-terminal part of the BC loop are disordered. Binding of azole inhibitors or estriol triggers ordering of the C helix in the 4-phenylimidazole bound form (Figure 4B) and partial ordering in fluconazole- and estriol bound forms (Figures 4A and 4B). Estriol binding restores one helical turn of the C helix. As a result of this transition, in the ligand-free form one of the heme propionates becomes exposed to the surface rather than being buried within the protein interior. Binding of azole inhibitors does not affect conformation of the BC loop. It remains stretched over the protein surface in both ligand-free and inhibitor bound forms. Binding of the estriol probe in the active site releases the BC loop from its position on the protein surface. The BC loop tends to relocate; however, it never orders enough to build continuous electron density in the estriol bound form, where the region 85–94 is represented by scattered electron density.

Although estriol mimics certain features of CYP51 substrates, it lacks the aliphatic side chain at C-17, which in this orientation of sterol in the active site would point toward the molecular surface, probably interacting with the BC loop and the C helix. We predict that these interactions would allow the BC loop to adopt a function-

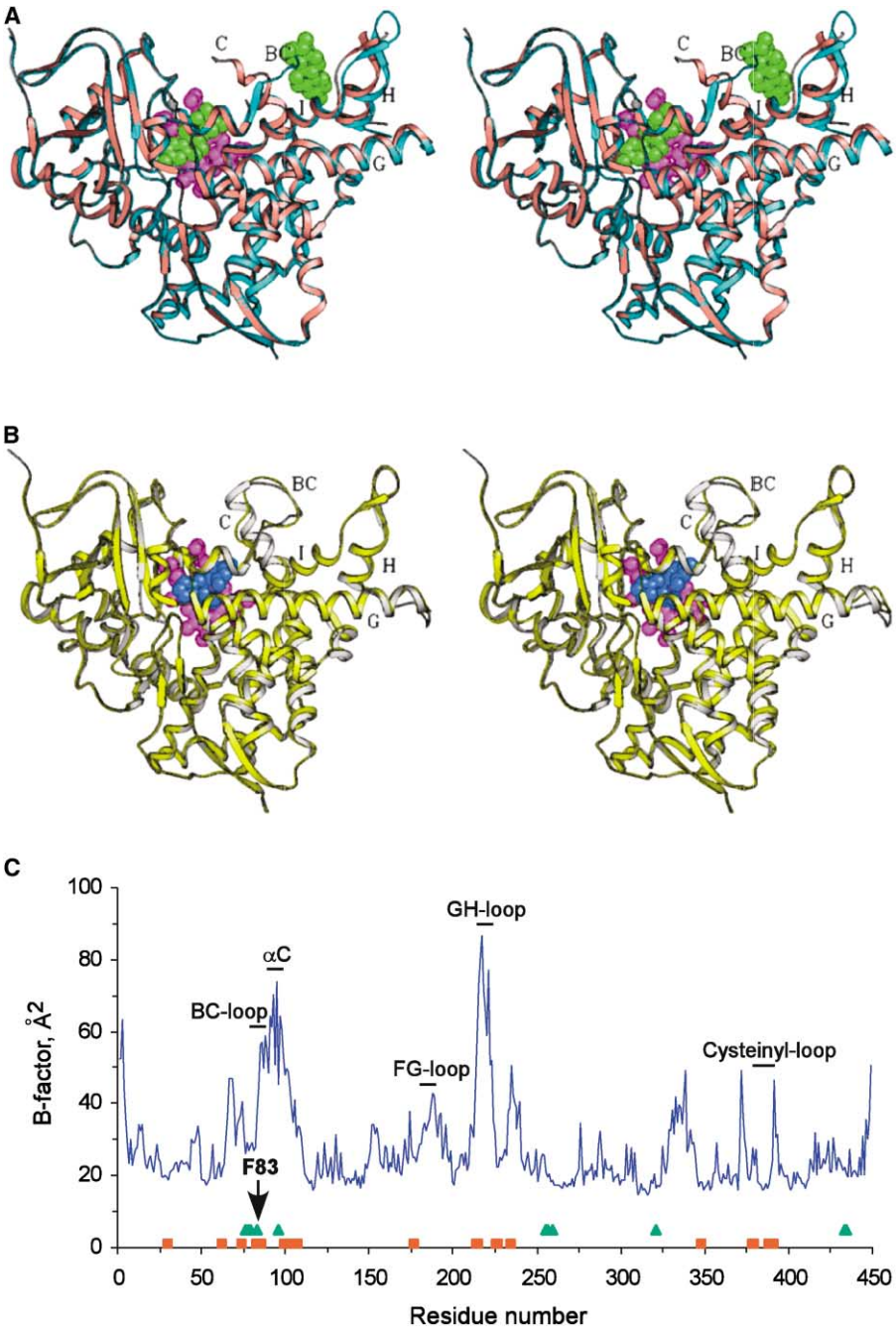

Figure 4. Stereoviews of MTCYP51 Structure in Different Forms

(A and B) Superimposition of the (A) ligand-free (cyan) and estriol bound (rose) and (B) 4-phenylimidazome bound (gray) and fluconazole bound (yellow) forms of the MTCYP51. Heme is shown in pink, estriol in green, and fluconazole in blue.

(C) Distribution of the estriol binding residues (green triangles) and mutations in azole-resistant clinical isolates of pathogen *C. albicans* (red squares) along MTCYP51 sequence. Plot shows temperature factors averaged per residue as they are observed in the 4-phenylimidazole bound form.

ally relevant closed conformation. Also, we assume that once substrate is bound in the active site, the guanidinium group of R96 would create stacking interactions with the unsaturated bond of the obtusifoliol side chain. Since CYP51 substrates are largely discriminated based on the structure of sterol side chain, it is not a surprise that this residue in CYP51 isoforms, with few exceptions, is phyla specific, being arginine in plant and most bacteria, methionine in low eukaryotes, leucine in yeast and fungi, and phenylalanine in vertebrates (Figure 5).

Estriol Binding and Substrate Specificity in CYP51

Estriol enters the MTCYP51 active site apparently with its 3β-hydroxy group leading through the opening created by the disordered C helix, bent I helix, and by the extended conformation of the BC loop, as was predicted

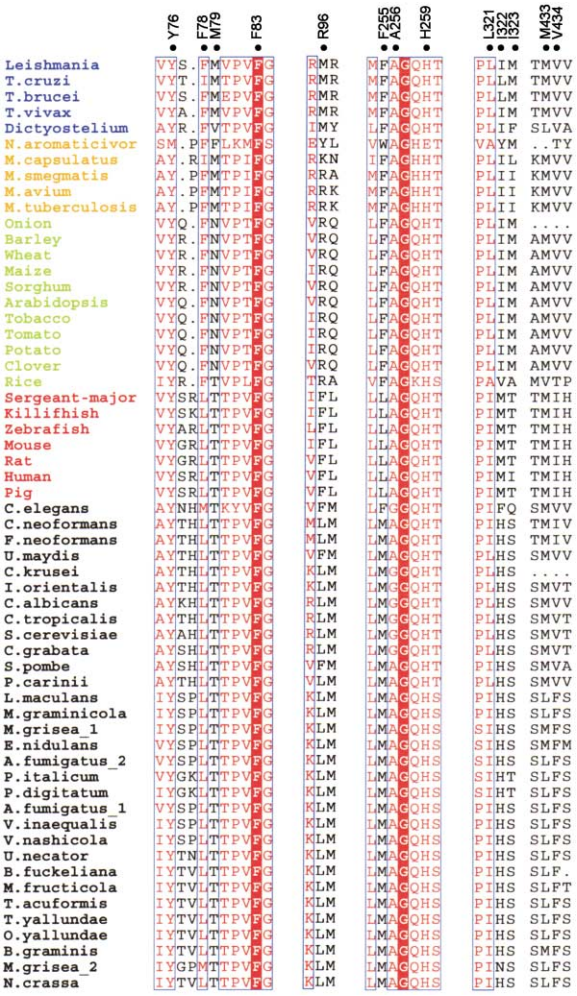

Figure 5. Estriol-Interacting Residues across Phyla

Fragments of multiple sequence alignment between 59 CYP51 isoforms from different organisms representing residues binding estriol in MTCYP51, noted by closed circles at top. Alignment performed using the MAP algorithm as implemented in the BCM Search Launcher (http://searchlauncher.bcm.tmc.edu/multi-align/multi-align.html).

based on molecular dynamic simulations (Podust et al., 2001b). Electron density for estriol is unambiguously defined (Figure 6B). The invariant 3β-hydroxy group of estriol does not hydrogen bond to any side chains in the active site, but instead is hydrogen bonded to the carbonyl oxygen of M433 and via an ordered water molecule to the amide nitrogen of I322 (Figure 6A). Additionally, the carbonyl oxygen of I323 is within 4.26 Å from the invariant OH-group of estriol and may contribute in a hydrogen bonding network either for estriol or for a natural substrate. Altogether, nine protein side chains are within 4.0 Å from estriol: Y76, F78, F83, F255, A256, H259, L321, M433, and R96. In addition, V434 and M79 are within 4.6 Å and might interact either with substrate methyl group(s) at C-4 (V434) or at C-10 (M79). Three (Y76, F83, and H259) of these eleven residues are invariant among all CYP51s (with the exception of *N. aromaticivorans*, which so far is the most remote relative in the CYP51 family) (Figure 5). Only one residue, F78, is specific for plant obtusifoliol-metabolizing CYP51s and for other CYP51s whose preference for obtusifoliol versus 4α,4β-dimethylated substrates was demonstrated in vitro, namely for *M. tuberculosis* (Bellamine et al., 1999) and *Trypanosoma brucei* (Lepesheva et al., 2004) CYP51. F78 is also present in a number of CYP51 isoforms whose substrate preferences have not yet been determined: *M. avium, M. smegmatis, Trypanosoma vivax, Leishmania major, Dictyostelium, and N. aromaticivorans*. F78 is a leucine in all other known CYP51 orthologs, except for proteobacterium *M. capsulatus* and low eukaryote *Trypanosoma cruzi* where it is an isoleucine, and for two fungi species where this residue is methionine. F78 is situated above the C-4 atom of estriol within only 3.76 Å and would directly interfere with the 4β-methyl group in 4α,4β-dimethylated CYP51 substrates (Figure 6C). As such, F78 is a candidate to be a key determinant of obtusifoliol selectivity in the CYP51 family. Thus, we would predict that all bacterial CYP51s listed in Figure 5, with the exception of *M. capsulatus*, would favor 4α-methylated substrate obtusifoliol versus 4α,4β-dimethylated substrates. Three out of four lower eukaryote CYP51s, the exception being *T. cruzi*, should also favor obtusifoliol.

Dynamics of CYP51 and Fluconazole Resistance

Estriol binds in the active site of MTCYP51 via the same set of residues as fluconazole, plus I323 and M433 interacting with the invariant 3β-hydroxy group. The movement of the side chains in this portion of the substrate binding site is minimal for all four MTCYP51 forms. Thus, this part of the binding site is preformed before binding. As has been discussed elsewhere (Podust et al., 2001a, 2001b), residues interacting with fluconazole in MTCYP51 do not overlap with the residues mutated in CYP51 in fluconazole-resistant strains of the most studied yeast pathogen, *C. albicans*, with the exception of F83 (Figure 4C). Instead, the majority of mutations identified in clinical isolates (Marichal et al., 1999; Morschhauser, 2002) flank the most dynamic regions of the MTCYP51, the C helix, the BC, and the GH loops. An exception is a mutation hot spot associated with the N-terminal part of the cysteinyl loop in the heme binding pocket, the hinge between β sheet and α-helical protein domains, which is not the most dynamically active region in the molecule (Figure 4C). Half of the *C. albicans* mutations mapped to this hot spot are substitutions of glycine to serine or glutamate, which should affect flexibility of the cysteinyl loop itself and probably interdomain conformational changes, if the latter should occur upon binding of substrate.

Comparison of ligand-free and ligand bound MTCYP51 structures indicates that remodeling of the C helix and the BC loop are required to "close the lid" and complete formation of the high-affinity substrate binding site of MTCYP51. Failure to close the lid would result in reduced affinity for the ligand. Considering a high level of conservation of residues involved in substrate binding within each phylum (Figure 5), we conclude that organisms cannot afford to change substrate-interacting residues in CYP51 to combat the effect of drugs without

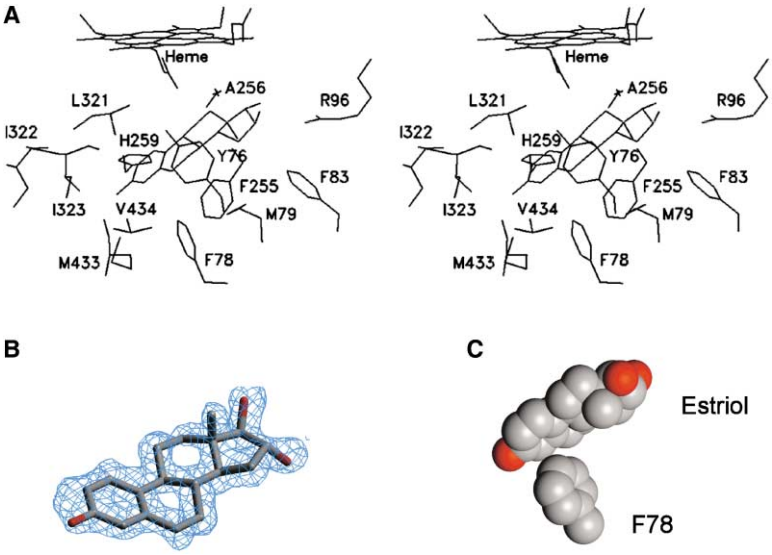

Figure 6. Estriol Binding in the Active Site of MTCYP51

(A) Stereo view of estriol bound in the active site of MTCYP51.

(B) Electron density for estriol represented by a fragment of the $2F_o$-F_c composite omit map contoured at 1.2σ.

(C) Estriol and F78 are represented by their van der Waals radii in the binding site of MTCYP51, in the same orientations as in stereo view (A).

interference in the physiological function of the enzyme, sterol biosynthesis. What might be allowed, though, is to modulate protein dynamics through mutagenesis of residues in fulcrum positions, which are not involved directly in interactions with substrate but which affect the protein's ability to perform required rearrangements, so that the lid does not close when an inhibitor binds, maintaining the low-affinity state, but it does close in response to substrate binding, leading to a higher-affinity state. We hypothesize that this is one of the mechanisms the pathogen *C. albicans* and probably other pathogens use to favor substrate versus inhibitor. Clearly, the residual affinity to the drug cannot be decreased by this mechanism below a background value, which is determined by the area of the preformed portion of the active site interacting with the drug. To combat infection more efficiently, one can increase the size of the inhibitor to cover a larger area. This approach has been utilized in development of second-generation antifungal triazoles such as voriconazole, ravuconazole, itraconazole, and posaconazole (Gupta and Tomas, 2003), which are all larger than fluconazole. In particular, the long side chain of itraconazole and posaconazole is likely to extend into the FG channel within CYP51 to provide additional interactions with the protein, as was modeled elsewhere based on the structure of MTCYP51 (Gollapudy et al., 2004; Xiao et al., 2004). However, this approach to drug design is limited by the size of the preformed binding area itself. Another approach, which, based on our knowledge, has not yet been exploited in antifungal drug design would be to mimic those substrate-protein interactions that trigger conformational changes leading to the lid closure. Apparently, the aliphatic side chain of the substrate would provide part of these interactions. The availability of a crystal structure of a substrate bound MTCYP51 could help refine our understanding of the specific contacts required for drugs to trigger the transition from the preformed lower-affinity binding site to the induced-fit higher-affinity one, which could push affinity of new drugs into a nanomolar range.

Experimental Procedures

Protein Design, Purification, and Analysis

MTCYP51 differs from the wild-type protein by addition of a 4× His tag at the C terminus. For cocrystallization with estriol, the double mutant C37L/C442A-MTCYP51 was used. Both forms were expressed in HMS174(DE3) (Novagen) *E. coli* strain at 20°C–25°C with an induction period of 20 hr. Purification on Ni^{2+} resin (Qiagen) was followed by flow-through chromatography on S-Sepharose (Amersham Pharmacia Biotech) and binding to Q-Sepharose (Amersham Pharmacia Biotech), from which MTCYP51 was eluted by NaCl gradient, 0–0.5 M. Protein was concentrated to 0.8 mM by using a Centricon YM-50 centrifugal device.

Purified wild-type and mutant MTCYP51 were analyzed by SDS-PAGE in the absence and presence of DTT in increasing concentrations. 0.5 μg of protein in 50 μl of SDS-sample buffer containing dithiothreitol (DTT), as indicated above each lane (Figure 1), was incubated for 5 min at 95°C. 3.5 μl from each sample was loaded onto 12.5% precast gels and run using the FastSystem (Amersham Pharmacia Biotech).

Heme content was estimated as a ratio between protein containing heme with P450 nm absorbance and total protein. Concentration of total protein was measured using the BCA Protein Assay Reagent (Pierce) according to the protocol provided by the manufacturer. Concentration of heme-containing protein was accessed by CO-reduced difference spectra based on the extinction coefficient of 91,000 $M^{-1}cm^{-1}$ (Omura and Sato, 1964).

Mass-Spectrometry Analysis of MTCYP51 Tryptic Digests

8 μg of MTCYP51 was digested with trypsin (Roche) in 100 μl of 50 mM ammonium bicarbonate using an enzyme/substrate ratio of 1:40 (w/w) at 37°C overnight. One-half of the tryptic digest was incubated with 5 mM DTT for 20 min at 70°C. 1 μl aliquots of the reduced and nonreduced tryptic digests were analyzed using a Protein Biology System II ProteinChip Reader, which is a surface-enhanced laser desorption/ionization time of flight (SELDI-TOF) mass spectrometer (Ciphergen Biosystems, Inc). α-cyano-4-hydroxy-cinnamic acid was used as the energy-adsorbing molecule, and the mass spectrometer was externally calibrated using an All-in-1 Peptide standard (Ciphergen Biosystems, Inc.). The experimental data were converted from m/z values and are reported as average molecular weights in Daltons.

Estriol Binding Assay

Estriol, 1,3,5(10)-estratrien-3,16α,17β-triol (Sigma)-induced spectral shifts were monitored at room temperature using a Shimazu UV-2401 spectrophotometer. Samples contained 5 μM MTCYP51 in 100

mM Tris-HCl (pH 7.5), 10% glycerol. Estriol was dissolved in DMSO at a stock concentration of 25 mM. K_d value was estimated using spectrophotometric titration by adding estriol in 1 μl aliquots to the sample and DMSO to the reference cuvette, followed by recording of difference spectra. Data were linearized in a $S_0/\Delta A$ versus S_0 plot, where S_0 is a total concentration of estriol in the reaction mixture.

Crystal Growth and Data Collection

Crystals were grown by vapor diffusion in a hanging drop, using 1:1 ratio of 0.2 mM protein in a solution of 10 mM Tris-HCl (pH 7.5), 50 mM NaCl against a crystallization well solution of 20% PEG4000, 10% isopropanol, 0.1 M Na cacodilate (pH 6.5) for ligand-free crystals and 25% PEG4000, 4% isopropanol, 0.1 M HEPES (pH 7.5) for estriol bound crystals. Lanosterol or estriol dissolved in acetone or alcohol, respectively, were added to the protein at 1–2 mM concentration prior to mixing with well solution. Crystals grew at 22°C (ligand free) and 20°C (estriol bound) over the course of a few weeks.

For data collection, crystals were briefly immersed into well solution containing 25% glycerol and flash cooled in liquid N_2. Data were collected using the laboratory source R-AXIS IV mounted on a RU-200 X-ray generator (Rigaku, Tokyo) and synchrotron radiation of the Southeast Regional Collaborative Access Team (SER-CAT) 22-ID beamline at the Advanced Photon Source, Argonne National Laboratory. The images were integrated and the intensities were merged using HKL2000 (Otwinowski and Minor, 1997). X-ray diffraction statistics are shown in Table 1.

Structure Determination and Refinement

Both ligand-free and estriol bound MTCYP51 structures were determined by molecular replacement by using as a search model the 4-phenylimidazole bound MTCYP51 structure (Protein Data Bank [PDB] ID code 1E9X) and CNS software (Brunger et al., 1998). CNS and SHELX (Sheldrick, 1990) were used for refinement, O (Jones et al., 1991) for manual model building, and PROCHECK (Laskowski et al., 1993) for model evaluation. The final model for the ligand-free form consists of residues 2–449 along with the heme group and 280 water molecules. Seventeen residues are omitted and four residues are substituted for Ala in the PDB entry because of insufficient electron density. The final model for the estriol bound form consists of residues 2–449 along with the heme group, two estriol molecules, and 323 water molecules. Twenty-two residues are omitted and two residues are substituted for Ala.

Acknowledgments

We thank Dr. Joel Harp for expert assistance in computation, Southeast Regional Collaborative Access Team (SER-CAT) Argonne National Laboratory for assistance with data collection, and Richard D'Aquila for critical reading of the manuscript and many useful suggestions. This work was supported by NIH grants GM37942, GM067871, and ES00267 (to M.R.W.), and P30 ES00267 and VUMC Discovery Grant Program (to L.M.P.).

Received: June 18, 2004
Revised: August 19, 2004
Accepted: August 23, 2004
Published: November 9, 2004

References

Aoyama, Y., Noshiro, M., Gotoh, O., Imaoka, S., Funae, Y., Kurosawa, N., Horiuchi, T., and Yoshida, Y. (1996). Sterol 14-demethylase P450 (P45014DM*) is one of the most ancient and conserved P450 species. J. Biochem. (Tokyo) *119*, 926–933.

Aoyama, Y., Horiuchi, T., Gotoh, O., Noshiro, M., and Yoshida, Y. (1998). CYP51-like gene of *Micobacterium tuberculosis* actually encodes a P450 similar to eukaryotic CYP51. J. Biochem. (Tokyo) *124*, 694–696.

Bellamine, A., Mangla, A.T., Nes, W.D., and Waterman, M.R. (1999). Characterization and catalytic properties of the sterol 14alpha-demethylase from *Mycobacterium tuberculosis*. Proc. Natl. Acad. Sci. USA *96*, 8937–8942.

Bird, C.W., Lynch, J.M., Pirt, F.J., and Reid, W.W. (1971). Steroids and squalene in *Methylococcus capsulatus* grown on methane. Nature *230*, 473–474.

Bode, H.B., Zeggel, B., Silakowski, B., Wenzel, S.C., Reichenbach, H., and Muller, R. (2003). Steroid biosynthesis in prokaryotes: identification of myxobacterial steroids and cloning of the first bacterial 2,3(S)-oxidosqualene cyclase from the myxobacterium *Stigmatella aurantiaca*. Mol. Microbiol. *47*, 471–481.

Brennan, P.J., and Nikaido, H. (1995). The envelope of *Mycobacteria*. Annu. Rev. Biochem. *64*, 29–63.

Brunger, A.T., Adams, P.D., Clore, G.M., Delano, W.L., Gros, P., Grosse-Kunstleve, R.W., Jiang, J.-S., Kuszewski, J., Nilges, M., and Pannu, N.S. (1998). Crystallography and NMR system: a new software suite for macromolecular structure determination. Acta Crystallogr. D Biol. Crystallogr *54*, 905–921.

Gollapudy, R., Ajmani, S., and Kulkarni, S.A. (2004). Modeling and interactions of *Aspergillus fumigatus* lanosterol 14-[alpha] demethylase 'A' with azole antifungals*1. Bioorg. Med. Chem. *12*, 2937–2950.

Gottesman, M.E., and Hendrickson, W.A. (2000). Protein folding and unfolding by *Escherichia coli* chaperones and chaperonins. Curr. Opin. Microbiol. *3*, 197–202.

Gupta, A.K., and Tomas, E. (2003). New antifungal agents. Dermatol. Clin. *21*, 565–576.

Houry, W.A., Frishman, D., Eckerskorn, C., Lottspeich, F., and Hartl, F.U. (1999). Identification of in vivo substrates of the chaperonin GroEL. Nature *402*, 147–154.

Jackson, C.J., Lamb, D.C., Marczylo, T.H., Warrilow, A.G.S., Manning, N.J., Lowe, D.J., Kelly, D.E., and Kelly, S.L. (2002). A novel sterol 14alpha-demethylase/ferredoxin fusion protein (MCCYP51FX) from *Methylococcus capsulatus* represents a new class of the cytochrome P450 superfamily. J. Biol. Chem. *277*, 46959–46965.

Jones, T.A., Zou, J.Y., Cowan, S.W., and Kjeldgaard, M. (1991). Improved methods for building protein models in electron density maps and the location of errors in these models. Acta Crystallogr. A *47*, 110–119.

Kohl, W., Gloe, A., and Reichenbach, H. (1983). Steroids from the myxobacterium *Nannocystis exedens*. J. Gen. Microbiol. *129*, 1629–1635.

Koltin, Y., and Hitchcock, C.A. (1997). The search for new triazole antifungal agents. Curr. Opin. Chem. Biol. *1*, 176–182.

Laskowski, R.A., MacArthur, M.W., Moss, D.S., and Thornton, J.M. (1993). PROCHECK: a program to check the stereochemical quality of protein structures. J. Appl. Crystallogr. *26*, 283–291.

Lepesheva, G.I., Podust, L.M., Bellamine, A., and Waterman, M.R. (2001). Folding requirements are different between sterol 14alpha-demethylase (CYP51) from *Mycobacterium tuberculosis* and human or fungal orthologs. J. Biol. Chem. *276*, 28413–28420.

Lepesheva, G.I., Nes, W.D., Zhou, W., Hill, G.C., and Waterman, M.R. (2004). CYP51 from *Trypanosoma brucei* is obtusifoliol-specific. Biochemistry *43*, 10789–10799.

Marichal, P., Koymans, L., Willemsens, S., Bellens, D., Verhasselt, P., Luyten, W., Borgers, M., Ramaekers, F.C.S., Odds, F.C., and Bossche, H.V. (1999). Contribution of mutations in the cytochrome P450 14α-demethylase (Erg11p, Cyp51p) to azole resistance in *Candida albicans*. Microbiol. *145*, 2701–2713.

Morschhauser, J. (2002). The genetic basis of fluconazole resistance development in *Candida albicans*. Biochim. Biophys. Acta *1587*, 240–248.

Omura, T., and Sato, R. (1964). The carbon monoxide-binding pigment of liver microsomes. II. Solubilization, purification, and properties. J. Biol. Chem. *239*, 2379–2385.

Otwinowski, Z., and Minor, W. (1997). Processing of x-ray diffraction data collected in oscillation mode. Methods Enzymol. *276*, 307–326.

Ourisson, G., and Nakatani, Y. (1994). The terpenoid theory of the origin of cellular life: the evolution of terpenoids to cholesterol. Chem. Biol. *1*, 11–23.

Park, S.Y., Yamane, K., Adachi, S., Shiro, Y., Weiss, K.E., Maves,

S.A., and Sligar, S.G. (2002). Thermophilic cytochrome P450 (CYP119) from *Sulfolobus solfataricus*: high resolution structure and functional properties. J. Inorg. Biochem. *91*, 491–501.

Pearson, A., Budin, M., and Brocks, J.J. (2003). Phylogenetic and biochemical evidence for sterol synthesis in the bacterium *Gemmata obscuriglobus*. Proc. Natl. Acad. Sci. USA *100*, 15352–15357.

Podust, L.M., Poulos, T.L., and Waterman, M.R. (2001a). Crystal structure of cytochrome P450 14α-sterol demethylase (CYP51) from *Mycobacterium tuberculosis* in complex with azole inhibitors. Proc. Natl. Acad. Sci. USA *98*, 3068–3073.

Podust, L.M., Stojan, J., Poulos, T.L., and Waterman, M.R. (2001b). Substrate recognition sites in 14alpha-sterol demethylase from comparative analysis of amino acid sequences and X-ray structure of *Mycobacterium tuberculosis* CYP51. J. Inorg. Biochem. *87*, 227–235.

Podust, L.M., Kim, Y., Arase, M., Neely, B.A., Beck, B.J., Bach, H., Sherman, D.H., Lamb, D.C., Kelly, S.L., and Waterman, M.R. (2003). The 1.92-A structure of *Streptomyces coelicolor* A3(2) CYP154C1. A new monooxygenase that functionalizes macrolide ring systems. J. Biol. Chem. *278*, 12214–12221.

Schouten, S., Bowman, J.P., Rijpstra, W.I., and Sinninghe Damste, J.S. (2000). Sterols in a psychrophilic methanotroph, *Methylosphaera hansonii*. FEMS Microbiol. Lett. *186*, 193–195.

Scott, E.E., He, Y.A., Wester, M.R., White, M.A., Chin, C.C., Halpert, J.R., Johnson, E.F., and Stout, C.D. (2003). An open conformation of mammalian cytochrome P450 2B4 at 1.6-A resolution. Proc. Natl. Acad. Sci. USA *100*, 13196–13201.

Scott, E.E., White, M.A., He, Y.A., Johnson, E.F., Stout, C.D., and Halpert, J.R. (2004). Structure of mammalian cytochrome P450 2B4 complexed with 4-(4-chlorophenyl)imidazole at 1.9-A resolution: insight into the range of P450 conformations and the coordination of redox partner binding. J. Biol. Chem. *279*, 27294–27301.

Sheehan, D.J., Hitchcoch, C.A., and Sibley, C.M. (1999). Current and emerging azole antifungal agents. Clin. Microbiol. Rev. *12*, 40–79.

Sheldrick, G.M. (1990). Phase annealing in SHELX-90: direct methods for larger structures. Acta Crystallogr. *A46*, 467–473.

Xiao, L., Madison, V., Chau, A.S., Loebenberg, D., Palermo, R.E., and McNicholas, P.M. (2004). Three-dimensional models of wild-type and mutated forms of cytochrome P450 14alpha-sterol demethylases from *Aspergillus fumigatus* and *Candida albicans* provide insights into posaconazole binding. Antimicrob. Agents Chemother. *48*, 568–574.

Yano, J.K., Koo, L.S., Schuller, D.J., Li, H., Ortiz de Montellano, P.R., and Poulos, T.L. (2000). Crystal structure of a thermophilic cytochrome P450 from the archaeon *Sulfolobus solfataricus*. J. Biol. Chem. *275*, 31086–31092.

Zerbe, K., Pylypenko, O., Vitali, F., Zhang, W., Rouset, S., Heck, M., Vrijbloed, J.W., Bischoff, D., Bister, B., Sussmuth, R.D., et al. (2002). Crystal structure of OxyB, a cytochrome P450 implicated in an oxidative phenol coupling reaction during vancomycin biosynthesis. J. Biol. Chem. *277*, 47476–47485.

Accession Numbers

The atomic coordinates have been deposited in the Protein Data Bank under ID codes 1H5Z and 1X8V.